Highlights

Mechanical characterisation of hand first dorsal interosseous muscle during gripping

Simon Vauthier, Christophe Noël, Nicla Settembre, Emmanuel Foltête, Jérôme Chambert, Emmanuelle Jacquet

- Development of an apparatus to capture FDI muscle mechanical behaviour while gripping.
- Investigating hyperelastic, viscoelastic and anisotropic behaviour of the FDI muscle.
- FDI muscle stiffness rises quasi-linearly with grip, mainly along longitudinal fibre.
- Grip and vibration frequency affect FDI muscle stiffness and dissipation.

Mechanical characterisation of hand first dorsal interosseous muscle during gripping

Simon Vauthier^{a,b}, Christophe Noël^{a,*}, Nicla Settembre^c, Emmanuel Foltête^d, Jérôme Chambert^b, Emmanuelle Jacquet^b

^aElectromagnetism, Vibration, Optics Laboratory, Institut national de recherche et de sécurité (INRS), 54500, Vandæuvre-lès-Nancy, France

^bUniversité de Franche-Comté, CNRS, Institut FEMTO-ST, F-25000, Besançon, France

^cDepartment of Vascular Surgery, Nancy University Hospital, University of Lorraine, Vandæuvre-lès-Nancy, 54500, France

^dSUPMICROTECH, CNRS, Institut FEMTO-ST, F-25000, Besançon, France

Abstract

Prolonged exposure to vibrations from handheld tools can result in various disorders. Understanding how vibrations propagate through the hand is a key area of research involved in preventing these disorders. Within this framework, it is essential to grasp the mechanical behaviour of hand intrinsic muscles, especially as their properties may change during gripping due to muscular contraction. In order to achieve this objective, a homemade setup was elaborated with a view to measuring the mechanical characteristics of the first dorsal interosseous (FDI) muscle, which is located between the thumb and index finger. The apparatus featured quasi-static indentation, dynamic mechanical analysis (DMA), and shear wave elastography to investigate muscle hyperelastic, viscoelastic, and anisotropic properties, respectively. Measurements were conducted on 27 volunteers with grip instructions

Email address: christophe.noel@inrs.fr (Christophe Noël)

^{*.} Corresponding author

ranging from 0 to 40% of their maximal grip strength. The use of repeated measures analysis of variance and the computation of cross-correlations between the proposed measurement techniques unveiled that grip forces significantly modulate the mechanical behaviour of the FDI muscle. In addition, our results emphasised that the FDI muscle stiffened as grip force increased, primarily in the direction longitudinal to muscle fibres. The muscle static stiffness also rose non-linearly with the indenter penetration, thus exhibiting the hyperelastic behaviour of living tissues. The muscle dynamic stiffness was found to be strongly reshaped by vibration frequencies. It remained roughly constant up to around 100 Hz (when no grip), then climbed steeply. Grip force revealed its greatest influence on the muscle dynamic stiffness for vibrations with frequencies ranging from 20 Hz to approximately 300 Hz: the greater the grip force, the higher the dynamic stiffness. Furthermore, the FDI muscle was shown to exhibit a four- to six-fold increase in mechanical power dissipation between 20 Hz and 80 Hz when the handle was gripped at the maximum tested force, in comparison to no grip. Elevating grip forces increased vibration dissipated power within the hand muscles, thereby arguably leading to what are possibly the foremost vibration-induced risks.

Keywords: Hand-arm vibration, Skeletal muscle, Voluntary muscle activation, Quasi-static indentation, Dynamic mechanical analysis, Shear wave elastography

1. Introduction

Prolonged exposure to hand-transmitted vibrations can result in musculoskeletal, vascular and neurological disorders (Bovenzi, 1990, Griffin, 2012a)

collectively referred to as hand-arm vibration syndrome. The risk of developing these pathologies depends on vibration features, i.e., largely corresponding to their amplitude and frequency (Griffin, 2012b), and on the additional factors including the level of grip force exerted by the operator on the handle (Chetter et al., 1997).

Evaluation of the biodynamic response of the hand-arm system in various exposure conditions was investigated experimentally to better understand the influence of grip force. Several studies to date have focused on acceleration and force measurements directly on the handle. They have shown that increased gripping results in a rise of quantities like driving point mechanical impedance (Lindenmann et al., 2022) and mechanical energy absorbed by the upper limb (Burström and Lundström, 1988). However, the types of measurements found in these previous studies only described the overall response of the hand. Local measurements have also been taken of mechanical impedance (Lundström, 1984) on different locations of the hand, acceleration transmissibility of the wrist and forearm (Pan et al., 2018), accelerationtransmissibility mapping of the dorsal face of the hand (Noël, 2011, 2017a) and dynamic stiffness (Noël, 2017b) on distal phalanges. All of these studies have drawn approximately the same conclusion: increasing the grip force leads to an elevation in the vibration transmitted into the hand. This effect appears at medium-low frequencies (above 50 Hz) and becomes more local in higher frequencies (above 100-200 Hz). Analyses measuring over 500 Hz remain rare and sometimes inconsistent (Dong et al., 2008, Adewusi et al., 2008). These inconsistencies can be partially attributed to noisy vibrations created by the connecting parts of the setup (Dong et al., 2008) and to inertial effects of the instrumentation (Wu et al., 2006) which became significant at high frequencies.

Although the measurements undertaken to date provide a link between gripping and vibration exposure, they do not fully explain the mechanisms within hand tissues that lead to these effects. Indeed, gripping occurs as a result of the coordinated contraction of the extrinsic, located in the forearms, and intrinsic muscles, located inside the hand (Riordan, 1995, Hirt et al., 2017). This results in the fingers compressing the superficial tissues, such as the skin, fat and muscles, on the object that has been tightened.

On the one hand, measurements (Noël, 2017b) and simulations (Wu et al., 2014) have demonstrated that this compression leads to tissue stiffening and increases its dissipation. These phenomena result in changing the biomechanical response of the phalange (Noël, 2017b, Wu et al., 2017) and the hand (Wang et al., 2022). On the other hand, muscle contraction also modifies the mechanical properties of the muscles themselves (Gennisson et al., 2010). There are 21 intrinsic skeletal muscles inside the proximal area of the hand (Hirt et al., 2017), all of which participate in its biodynamic response. As a consequence, the grip force may also affect vibration transmission through muscle contraction. Furthermore, skeletal muscles consist of cells that are arranged around muscle fibres. It provides them with transverse isotropic properties, oriented according to the direction of the fibre bundles (Morrow et al., 2010, Gennisson et al., 2010). In addition, muscles exhibit hyperelastic (Gras et al., 2012) and viscoelastic (Wheatley et al., 2016) behaviour.

To date, no experimental studies have focused on the effect of gripping on the mechanical behaviour of intrinsic muscles. This lack of experimental data has also limited the development of numerical models. Even complex models of the hand still consider muscles in an undifferentiated way from other soft tissues (Wang et al., 2022, Liu et al., 2020).

To overcome these limitations, we aimed to design an experimental apparatus for characterising—as a function of gripping—the static stiffness, the viscoelastic properties and the anisotropy of an intrinsic muscle: the first dorsal interoseous (FDI) muscle. The FDI muscle is a bipennate muscle located between the first and second metacarpal bones; it contributes to gripping by abducting the index finger and opposing the thumb (Bilbo and Stern, 1986, Infantolino and Challis, 2010). Its superficial position beneath the dorsal face of the hand makes it relatively convenient for measurement while handling. Our strategy was to combine and adapt three measurement techniques used to characterise human tissues: quasi-static indentation, dynamic mechanical analysis (DMA) and shear wave elastography.

Quasi-static indentation involves driving a small probe onto the surface of a medium and measuring the resulting forces. It was used to characterise in vivo superficial tissues such as skin, flesh and muscles (Khaothong, 2010, Pailler-Mattei et al., 2008, Noël, 2017b). By largely deforming the medium, this technique emphasises the medium's hyperelastic behaviour. Furthermore, the measurement data were suitable for deducing the mechanical parameters of constitutive laws through inverse methods (Krajnak et al., 2012, Noël, 2018) or contact theories (Khaothong, 2010, Zahouani et al., 2009). DMA allows to investigate how the viscoelastic properties of a material evolve with frequency by subjecting that material to a cyclic excitation (Chatelin et al., 2011). For the characterisation of biological tissues in vivo,

the cyclic load is usually applied with an indenter probe moved by an electrodynamic shaker (Boyer et al., 2007, Noël, 2017b). However, the loaded region is generally a complex multi-layered medium and the muscle is not directly observable when placing the probe on the skin. As a consequence, both quasi-static indentation and DMA only give an overall response of the system, regardless of muscular fibre direction. Moreover, DMA requires prestressing the medium, which might affect measurements (Noël, 2017b). Yet shear wave elastography provides a local and directional measurement of the shear modulus inside muscles, and without prestressing the medium, but it requires linear-elasticity assumptions (Gennisson et al., 2010). In particular, the supersonic shear imaging (SSI) technique, derived from shear wave elastography, consists of focusing successively remote radiation pressures inside the muscle with a specific ultrasound probe generating spherical waves. The interferences between these waves result in a quasi-plane shear wave recorded at several kHz by the probe transducers (Gennisson et al., 2013). The shear modulus is then deduced from the wave group speed assuming the medium is linear and non-dispersive (Gennisson et al., 2010). By rotating the probe and measuring the shear modulus in different directions relative to the muscle fibres, it is possible to determine anisotropic material properties (Gennisson et al., 2010). In addition, SSI requires lighter instrumentation compared to other imaging techniques as magnetic resonance elastography (Ghatas et al., 2021) or optical elastography (Kearney et al., 2015) and is suitable for measurements in constrained environments such as the hand (Bouillard et al., 2011).

In conclusion, our study aims to address the gap in understanding the me-

chanical behaviour of intrinsic hand muscles during gripping. While previous research has explored the effects of gripping on overall hand biomechanics with a limited frequency bandwidth, this work seeks to describe the anisotropy, hyperelasticy and viscoelasticity of the FDI muscle while gripping. An ad hoc apparatus has been developed to take the required measurements from a group of volunteers: (i) static stiffness with quasi-static indentation; (ii) dynamic stiffness and dissipated mechanical power upon 2000 Hz with DMA; and (iii) longitudinal and transverse shear moduli with ultrasonic elastography. Through this study, we aim to provide insights into the biomechanical mechanisms underlying the interaction between gripping and muscle mechanical behaviour. This knowledge could facilitate the development of more accurate numerical models and contribute to a deeper understanding of prevention strategies for reducing hand-arm vibration syndrome.

2. Materials and methods

2.1. Apparatus

The test bench was designed so that a subject could stand in a posture that closely resembles that depicted in vibration measurement standard (ISO 10068:2012, 2012) while leaving the FDI muscle accessible for measurements (Fig. 1). The apparatus is divided into 3 distinctive parts: grip (Fig. 1a, items a to d), indentation (Fig. 1b) and elastography (Fig. 1c).

The gripping part consisted of an aluminium handle, made up of two half cylinders, each measuring 40 mm in diameter, into which two compression load cells (model Omega LCM201-500N) were inserted (Fig. 1a, item d). These sensors were connected to two different acquisition cards: one for

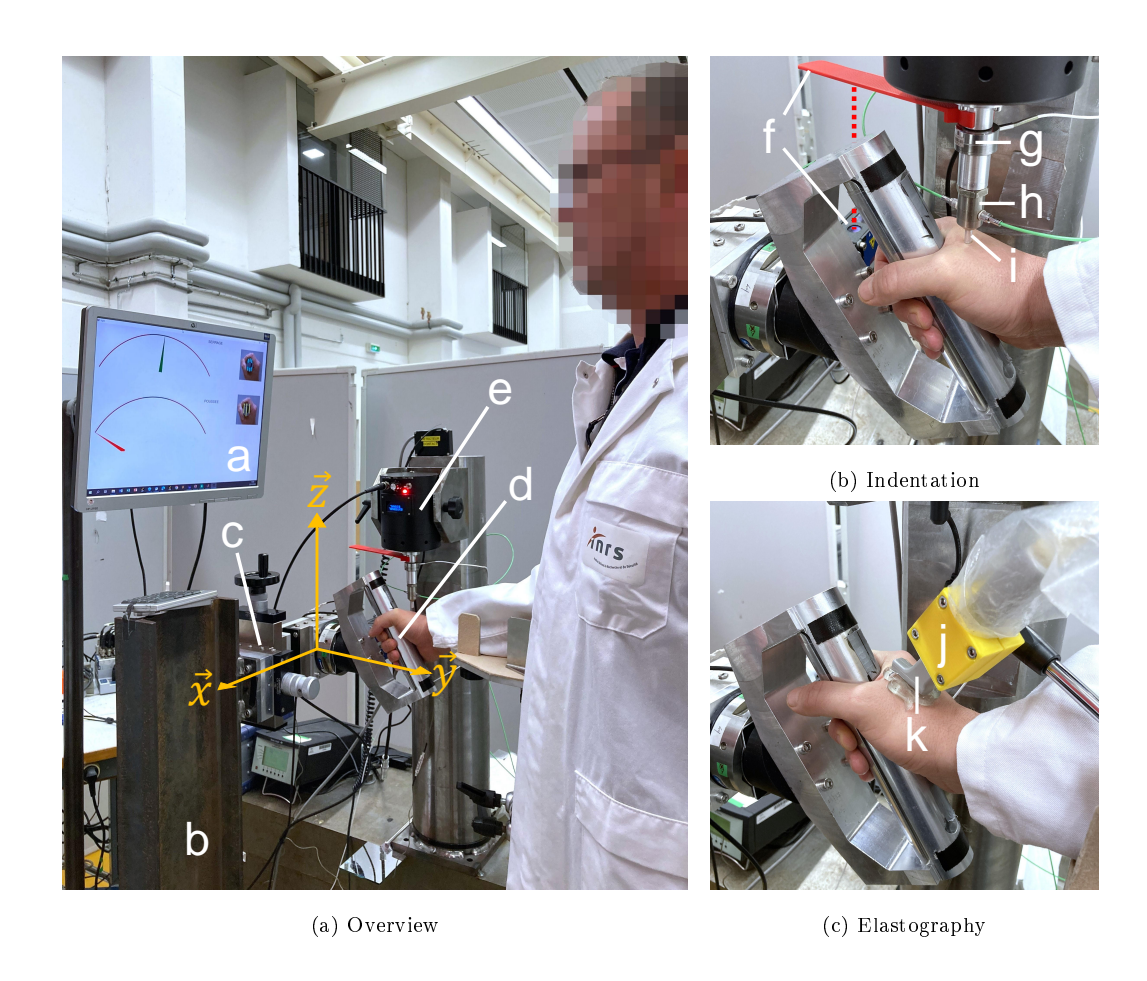


FIGURE 1 – Experimental apparatus : a) force gauge, b) I-beam, c) positioning table, d) instrumented handle, e) shaker f) telemeter and target g) piezoelectric force sensor, h) impedance head, i) indenter, j) probe holder, k) ultrasound probe.

recording the exerted grip force (module NI-9239); and one for displaying this to the subject in real time (self-made based on an Arduino[®] board). The immediate grip force was observable via a needle displayed on a screen facing the subject (Fig. 1a, item a). The cylindrical part of the handle was surrounded by a plastic film to protect the sensors from shear constraints. The handle was attached to a micrometre-driven positioning table ensuring a 100 mm displacement range among three orthogonal axes depicted on Fig. 1a, item c. The table was operated manually. The connecting piece between the table and the handle leaned it at $+30^{\circ}$ around the \vec{x} -axis. This ensured that the measurement zone—between the metacarpals of the thumb and index finger—was as horizontal as possible (Fig. 1b). The table was fastened to a metal I-beam (Fig. 1a, item b) clamped to a concrete base.

The indentation part was located on the upper right of the subject. The relevant instrumentation was mounted on the moving shaft of an electrodynamic shaker (Fig. 1a, item e and Fig. 1b). An aluminium hemispherical indenter, which was 5 mm in diameter (Fig. 1b, item i), was attached to its lower end. To avoid noise generated by vibration feedback during high-frequency measurements, the shaker was mounted on a 2 tonne cast-iron support, clamped to the concrete base mentioned above. The concrete base was isolated from the rest of the building and dedicated to vibration measurements. To perform static measurements, a piezoelectric force sensor (model B&K 8200) was screwed on the moving shaft (Fig. 1b, item g). To measure the relative displacements along \vec{z} -axis between the hand (linked to the handle) and the indenter (linked to the shaft), a laser telemeter (Micro-Epsilon optoNCDT 2300) was attached to the handle and aimed at a removable target onto the

shaft (Fig. 1b, item f). Both sensors were connected to an acquisition card, module NI-9239 (NI stands for National Instrument). For dynamic measurements, the target was removed to prevent unwanted oscillations. Dynamic force and acceleration were measured using an impedance head (model B&K 8001) located upon the indenter (Fig. 1b, item h). The sensors were connected to an acquisition card, module NI-9234. For both quasi-static and dynamic measurements, the detection of contact between the indenter and the skin was crucial to limit initial displacement offsets. Accordingly, the system was equipped with a low-amperage electrical device lightening when the indenter came into contact with the skin. To enhance electrical conductivity and reduce friction, the skin was moistened with water-based gel before quasi-static and dynamic indentation measurements were taken.

Elastography measurements were performed using an ultrasonic scanner SuperSonic Imagine™Aixplorer® equipped with a SuperLinear™SLH20-6 probe (Fig. 1c, item k) in SSI mode. In order to ensure the experimenter's access, the scanner was positioned behind the subject at the right of Fig. 1a (not visible). The probe was placed over the measurement zone with a layer of ultrasound gel a few millimetres deep and held with an articulated support, magnetised on the cast-iron base (Fig. 1c). During elastography measurements, the shaker was rotated so that the moving shaft was facing upwards, ensuring accessibility of the FDI muscle for the probe.

With the exception of the elastography acquisition, which was carried out directly on the scanner, all data acquisition, control and computations were performed using Matlab® software (version R2023a). Additionally, a lightweight specific software was developed in VB.NET to ensure a quick

response delay for live display of the grip force. All NI-acquisition cards were slotted into a chassis cDAQ-9174. The static and dynamic indentation devices were tested with calibrated springs, foams and mass to ensure their accuracy beforehand.

2.2. Protocol for the volunteers

This work was submitted to and approved by the French National Ethical Research Committee (CPP 22.03423.000122, 07/11/2022) and declared to the French National Agency for Medicines and Health Products (No. ID-RCB 2022-A01616-37, 07/11/2022). Written informed consent from each volunteer was obtained in accordance with the regulations of these organisations.

Twenty-seven volunteers (14 males and 13 females) aged between 19 and 36 years old (mean age was 23 years old) participated in the measurement campaign. All participants were healthy and non-smokers.

The protocol for the volunteers was consistent across the quasi-static, dynamic and elastography measurements. Volunteers stood facing the handle with their right elbow bent at approximately 90° to grip the handle. At each measurement, a grip instruction and experimental parameters were randomly selected. The target force was shown as a green gauge reachable by adjusting the force needle (Fig. 1a, item a). Volunteers had to keep the needle inside the gauge during the entire duration of measurement: approximately 30 seconds for indentation testing and less than 15 seconds for elastography. In the case of zero-gripping instruction, volunteers had only to position their hand without applying any force.

Instructions were provided as a percentage of the volunteers's maximum voluntary (MV) grip force. For measuring the MV grip force, volunteers as-

sumed the posture depicted in Fig. 1a and were instructed to gradually grip the instrumented handle until they reached their maximum force, and then released it. The maximum recorded force was stored and used to compute all subsequent instructions.

To prevent fatigue, a one-minute break was imposed between each measurement and 10-minute breaks between each of the three types of measurement.

During the entire measurement campaign, grip deviation remained below $\pm 1.5\%$.

Before doing the real measurements, an initial phase of learning with arbitrary instructions was operated. In parallel, the volunteers' posture was set by adjusting the position of the foot platform, the handle and the armrest. Particular attention was given to finding a stable and comfortable position to prevent unnecessary movements and fatigue during gripping. Once the position was set, marks were drawn on the floor, on the handle and on the hand to ensure identical positioning for each measurement.

2.3. Quasi-static stiffness measurements

Once the volunteers had reached the instruction level, the indenter probe was positioned flush with the skin, lighting up an LED. The laser telemeter was then reset to zero before moving the handle upwards using the crank, which resulted in the indenter moving forward onto the skin. The indenter displacement and the resulting force were recorded at a frequency of 2000 Hz. A Matlab® program computed the indenter speed in real-time and displayed it to the experimenter. The experimenter was able to track a speed reference of 0.5 mm/s, settled empirically as a compromise between maintaining a low

speed to avoid deviation from static hypotheses and keeping measurement time acceptable for the subjects. The final target displacement was 8 mm. Consequently, the acquisition time was approximately 16 s. The experimenter started and ended manually the acquisition, and subsequently trimmed the temporal displacement and force signals.

Computing the static stiffness K_s as the derivative of reaction force with respect to indenter displacement required force-displacement signals being differentiable. In order to achieve this, both signals were filtered using a SAVITZKY-GOLAY filter (Schafer, 2011) and initial offsets were suppressed. The filtered force-displacement curve was then fitted with an exponential sum of degree 2 (4 fitted parameters) using the least-square method. The static stiffness K_s was finally computed using numerical differentiation.

Static stiffness measurements were carried out at 0, 10, 20, 30 and 40% of MV grip force, repeated three times and averaged over repetitions. Regarding the quality of the exponential fit, the averaged R^2 -value over all measurements was above 0.99.

2.4. Definition of a prestressing criterion

DMA requires that material is constrained beforehand, usually at an iso-displacement or iso-compression rate. In our study, a compression rate could not be used because the deformation fields were unknown and a constant displacement level does not account for inter-subject variability. To tackle the problem, an iso-stiffness criterion, based on the quasi-static measurements, was chosen. For each grip instruction, an initial supposedly elastic stiffness K_s^0 was calculated by averaging the static stiffness K_s between 0 an 0.5 mm. Three prestressing criteria were then defined as $1.25 \cdot K_s^0$, $1.5 \cdot K_s^0$ and $2 \cdot K_s^0$

 K_s^0 . These values were empirically determined in order to achieve a balance between the necessary prestress, which is essential for ensuring measurement quality, and the limitation of prestress influence on dynamic measurements. Multiple prestressing conditions were chosen to investigate their potential effects on dynamic stiffness.

2.5. Dynamic stiffness measurements

The procedure for aligning the indenter with the skin and prestressing the muscle followed the same steps as described in section 2.3; only the target displacements differed. These corresponded to the penetration required to achieve the stiffness level defined by the prestressing criteria (Sec. 2.4). After applying the prestress, the telemeter target was removed (Fig. 1b, item f). During the dynamic measurements, acceleration and force were recorded at a sampling frequency of 5120 Hz. To obtain a controlled acceleration spectrum as input, the impulse response of the electrodynamic shaker between voltage and acceleration was calculated. This was done by exciting the indenter with white noise in voltage for 3 s, and then computing the voltage signal corresponding to the target acceleration using the method outlined by Noël (2017b). Next, the skin was excited with the computed voltage for 3 s. Three levels of acceleration a were tested: 5, 10 and 20 m/s² root mean square (rms). This procedure was repeated for each random set of grip instruction, each prestress criterion, and each acceleration level.

The complex dynamic stiffness $K_d(\nu)$ was computed as a function of frequency ν using the cross-spectrum method (Noël, 2017b):

$$K_d(\nu) = -(2\pi\nu)^2 \frac{S_{F,a}(\nu)}{S_{a,a}(\nu)}$$
 (1)

in which $S_{F,a}(\nu)$ is the cross-power spectral density between force F and acceleration a, and $S_{a,a}(\nu)$ is the power spectral density of acceleration a. The dissipated mechanical power generated by the force at the indenter end $\mathcal{P}_{\text{ext}}(\nu)$ was calculated as Noël (2017b):

$$\mathcal{P}_{\text{ext}}(\nu) = \frac{a_0^2}{2(2\pi\nu)^3} \Im(K_d(\nu)) \tag{2}$$

in which a_0 is the rms value of the acceleration a and $\Im(z)$ is the imaginary part of the complex number z.

2.6. Elastography measurements

Firstly, a substantial layer of ultrasound gel was applied beforehand to prevent the probe from compressing the skin. Subsequently, the probe was positioned and oriented approximately either parallel or perpendicular to the muscle fibre using the articulated support. Fine adjustments were made using the positioning table and the conventional B-mode imaging (Fig. 2, greyscale background). The volunteer then followed the grip instruction. Yet, the contraction of the FDI muscle could induce deformations within the tissues, necessitating additional adjustments. Thereafter, an SSI sequence was operated directly on the scanner, generating a DICOM®-format file, which was post-processed in a shear-elastic-modulus map (Fig. 2, colour foreground) using Matlab® routines. The shear modulus was then averaged within a region-of-interest (ROI). The position and diameter of ROI were chosen to find a homogeneous area without skin or nerves. The diameter ranged from 2 mm to 7 mm.

For each orientation, elastography measurements were carried out at 0, 5, 10, 15, 20, 30 and 40% of the MV grip force, repeated three times and

averaged over repetitions. If the probe was oriented parallel to the fibre, the longitudinal shear modulus of the muscle was deduced, while if it was oriented perpendicular to the fibre, the transverse shear modulus was deduced (Royer et al., 2011).

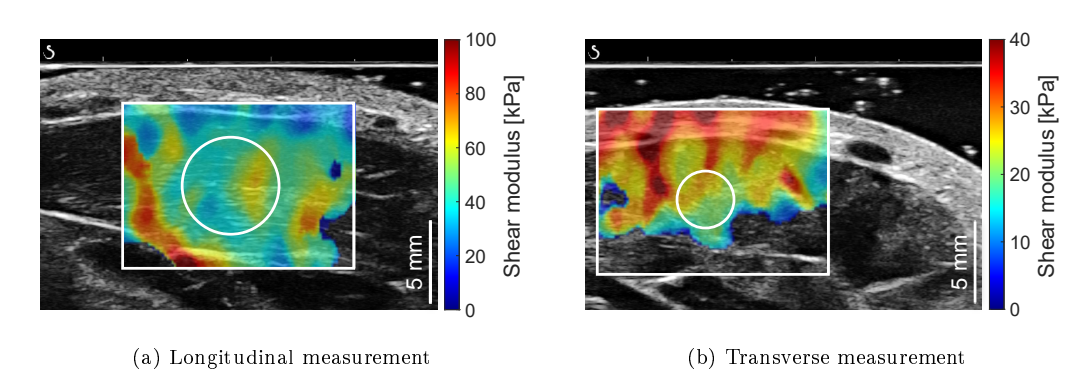


FIGURE 2 – Selection of an averaging ROI: greyscale background is the B-mode imaging, colour foreground is the shear-modulus mapping, white circle is the averaging ROI.

2.7. Statistical analysis

Pairwise correlation coefficients were computed for each subject, among grip levels, between longitudinal and transverse moduli, between longitudinal modulus and initial static stiffness, and between initial static stiffness and dynamic stiffness modulus at the lowest frequency (20 Hz). Repeated measurements of variance (RANOVA) using Lower bound adjustment were carried out for each type of measurement. Multiple comparisons of the estimated marginal means were performed using Tukey's honest significant difference procedure. A p-value of less than 0.05 was considered statistically significant.

3. Results

3.1. Longitudinal and transverse shear modulus measured by elastography

Fig. 3 shows the evolution of the elastic shear modulus averaged among volunteers with respect to the grip force for both directions of measurement. There were no significant differences between the longitudinal and transverse modulus before 5% gripping. In the longitudinal direction, all groups were significantly different from each other. Conversely, in the transverse direction, only the 0% grip was significantly different from all other levels of grip force. Those groups showed significant differences only with larger gaps in grip force : 5% with 20% and higher; 10% with 20% and higher; 15% with 30%; and 20% with 40%.

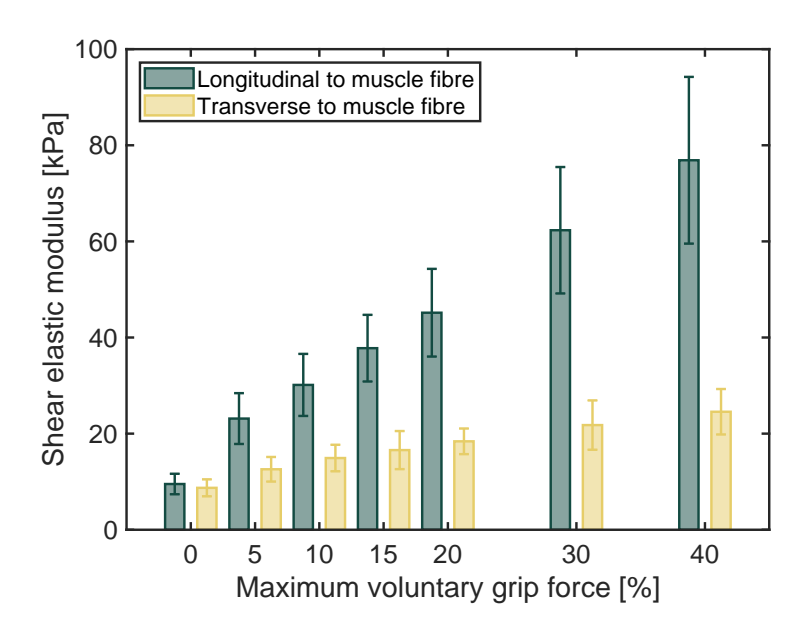


FIGURE 3 – Effect of grip force over the shear modulus averaged among volunteers; error bars depicts 95%-confidence intervals.

It was observed that the lower contraction level, at 5% grip force, resulted in a sudden rise in longitudinal modulus from the no-grip state. Beyond 5% grip force, longitudinal and transverse moduli appeared to increase quasi-linearly with grip force. For both directions, linear regression was computed over the subject-averaged modulus and exhibited R^2 value greater than 0.99. With regards to grip force, the longitudinal modulus showed a slope that was 4.5 times steeper than that of the transverse modulus. For a few volunteers, the longitudinal modulus reached a plateau at the highest grip forces.

3.2. Static stiffness obtained by quasi-static indentation

The force-displacement curves and the static stiffness-displacement curves, averaged among volunteers, are depicted in Fig. 4 for the five tested grip forces. Static stiffness was found to be strongly dependent on both indenter displacement (related to the applied strain) and the level of grip force. RANOVA calculation revealed that grip force was statistically significant regardless of displacement (p-value < 0.0001). Furthermore, results of the multiple comparison test indicated that each level of grip force was significantly different from the (p-value < 0.0001). The general shape of the forcedisplacement curve was consistent across all grip forces. At first, force steadily increased with displacement at low penetration (until 1 to 2 mm), before it rose exponentially with displacement. In terms of stiffness effects, the grip force multiplied the quasi-static stiffness by an approximate constant along the penetration range with respect to the no-grip state: from three times at 10% grip to seven times at 40%. The averaged stiffness was multiplied by approximately seven for all grip forces across the displacement range (from 6.7 at 40% to 8.7 at 0%) and doubled every 3 mm-displacement or so.

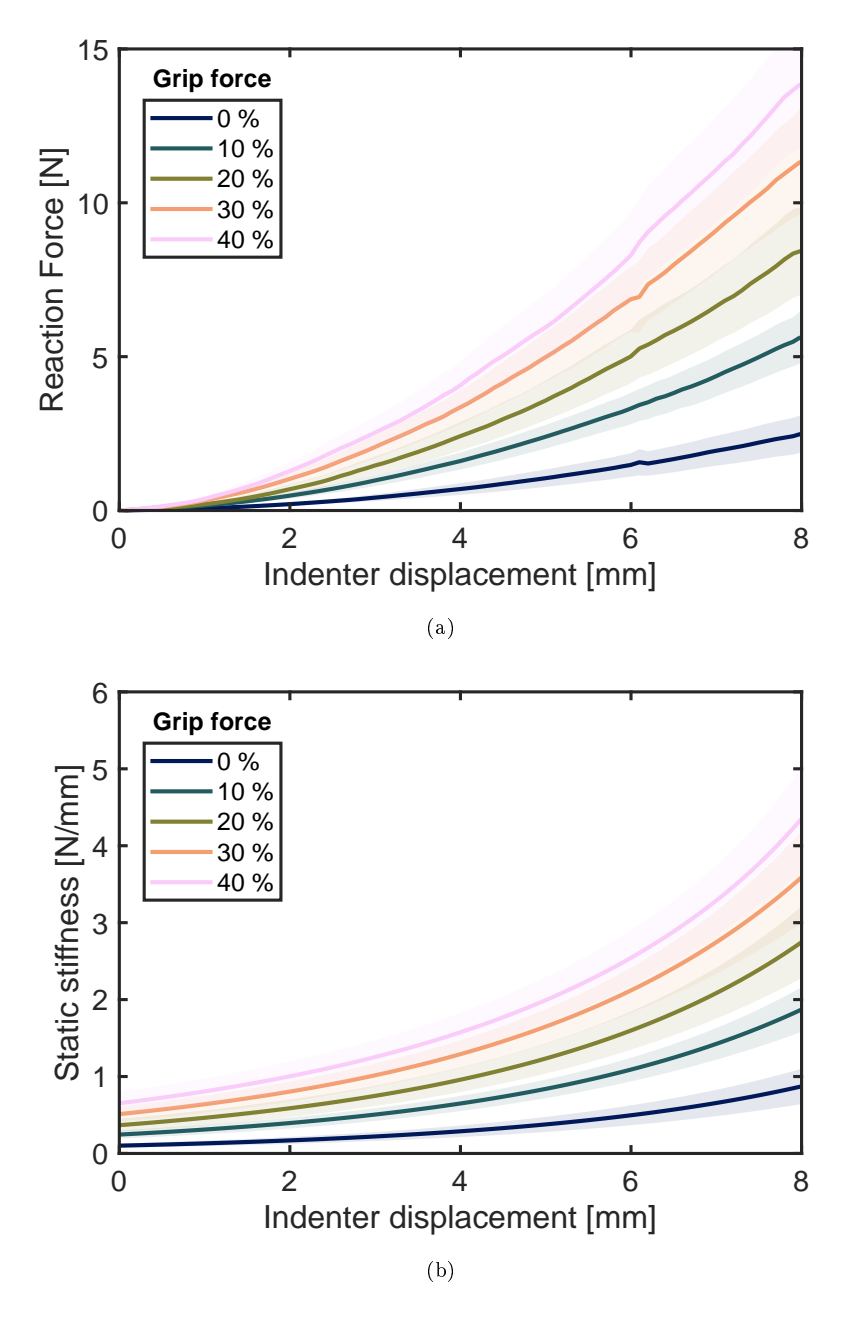


FIGURE 4 - Quasi-static indentation results : (a) averaged force-displacement curves among volunteers (b) averaged stiffness-displacement curves among volunteers; transparent patches are 95%-confidence intervals.

3.3. Dynamic stiffness obtained by dynamic indentation

Fig. 5 illustrates the statistical effects across several frequency ranges of grip force, applied prestress and imposed acceleration over the three computed quantities: the modulus and the phase angle of the dynamic stiffness; and the dissipated power. The frequency bands were chosen to correspond to the main classes of vibrating tools. Grip force and prestress appeared to be statistically significant for all measurements, regardless of frequency. Acceleration was also statistically significant, particularly on the phase, though it generally presented higher p-values. Beyond 1000 Hz, acceleration ceased to be significant for both stiffness modulus and dissipated power.

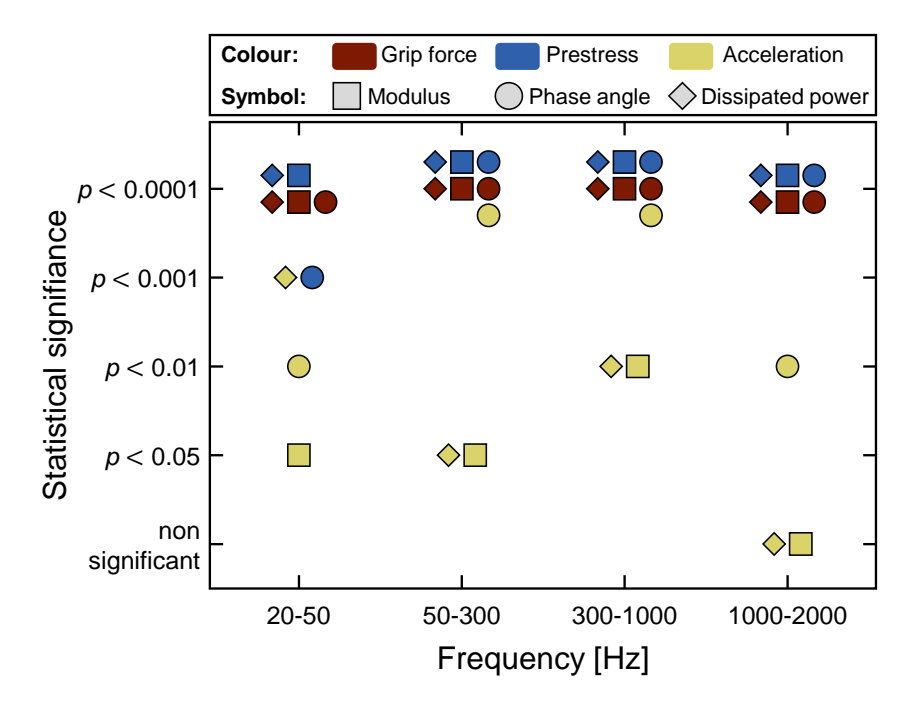


FIGURE 5 – Effect of grip force, prestress and acceleration on dynamic stiffness modulus, phase angle, and dissipated power; p is the statistical p-value.

The evolution of dynamic stiffness modulus and phase angle in relation to

frequency demonstrated a consistent trend across the range of tested parameters and variability among volunteers. Fig. 6 presents the dynamic stiffness averaged over volunteers at $1.5 \cdot K_s^0$ prestress and 20 m/s^2 rms acceleration. As the averaging process tends to smooth singular points, so the stiffness of a volunteer was plotted in dotted line to illustrate more clearly the shape of measurements. At low frequency, the modulus exhibited a flat concave shape up to a local minimum with an inflection point around 100 Hz. Over the next hundreds Hz, the curve rapidly increased to a local maximum, inflecting to a second local minimum and sharply raised again. Finally, the slope dropped progressively towards an oblique asymptote. Phase angle remained almost constant around 15° at the lowest frequencies. At the frequencies of modulus local minima, it showed two successive steep rises, split by an inflexion at the frequency of the modulus local maximum. Finally, the phase slowly reached a plateau region at around 100° .

Upon the first local minimum, grip force showed its greatest effect. On average, in the low-frequency band the 40% modulus was six to nine times stiffer than the no-grip state. Towards this point, grip effect steady decreased—in contrast with the influence of frequency—and converged with modulus asymptotic tendency. Beyond 1000 Hz, the 40% modulus remained twice as stiff as the no-grip state. At high frequencies, each grip force was not always statistically different from all the others, with the exception of the no-grip condition. Grip force also demonstrated complex influence inside the local-extremum area observable on both modulus and phase angle. On average, a 10% increase in grip force resulted in a frequency shift between 30 to 80 Hz of the first local minimum. In addition, the length and height of extreme

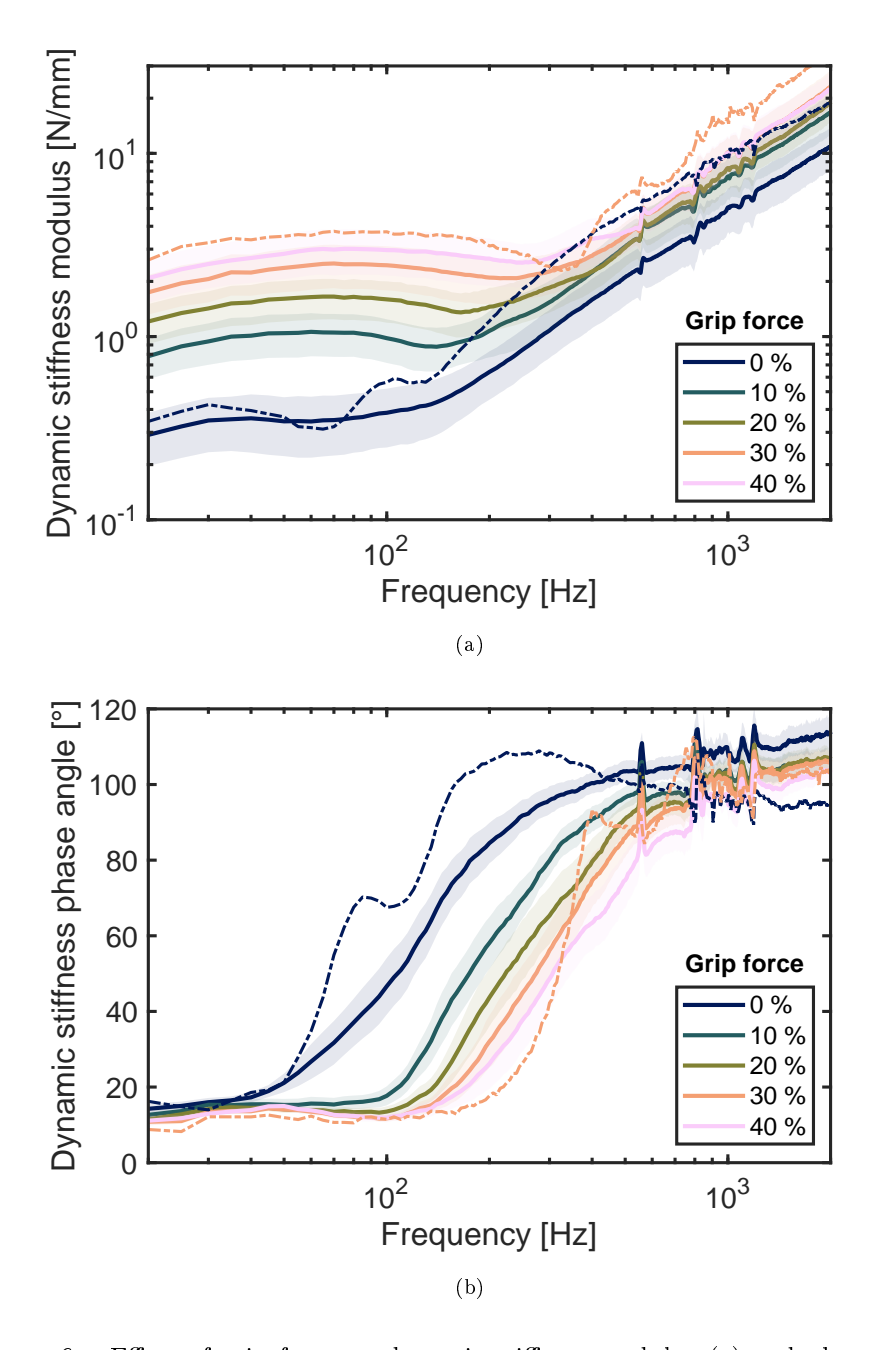


Figure 6 – Effect of grip force on dynamic stiffness modulus (a) and phase angle (b) averaged among volunteers; acceleration = $20~\rm m/s^2$, prestress = $1.5 \cdot K_s^0$; transparent patches are 95%-confidence intervals; dotted lines are specific-subject values.

peaks seemed to be modified by gripping but these phenomena could not be quantified among volunteers.

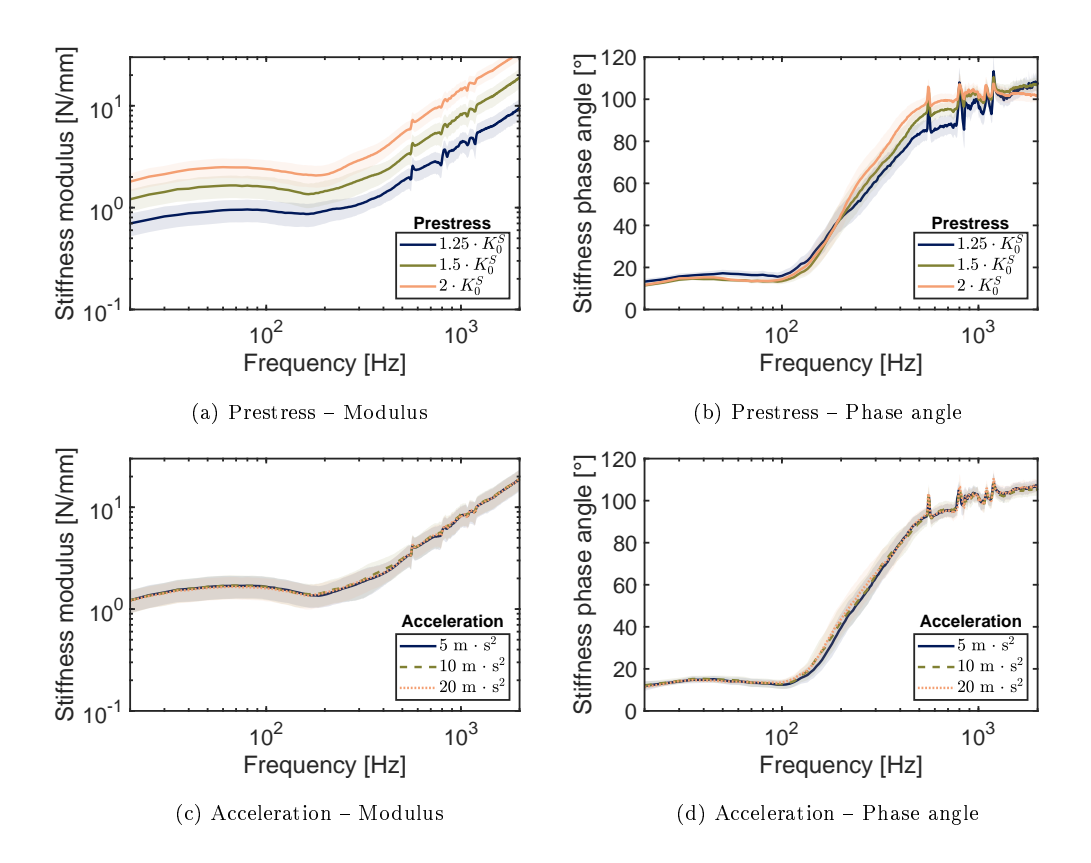


FIGURE 7 – Effect of prestress on dynamic stiffness modulus (a) and phase angle (b) averaged among volunteers at acceleration = $20~\rm m/s^2$ and grip force = 20%; effect of acceleration on dynamic stiffness modulus (c) and phase angle (d) averaged among volunteers at prestress = $1.5 \cdot K_s^0$ and grip force = 20%; transparent patches are 95%-confidence intervals.

Prestress had a marked but relatively simple effect on module and phase angle (Fig. 7a and Fig. 7b). Regarding the $1.25 \cdot K_0^S$ -prestress measurements, the intermediate-prestress multiplied the low-prestress stiffness by approximately 1.5 regardless of acceleration, gripping and frequency. The highest

prestress doubled it upon the first modulus local maximum and multiplied it by 2.5 to 3 beyond this frequency. Acceleration had a statistically significant effect on the stiffness modulus but its influence on amplitude was nearly negligible compared to the effects of prestress and grip force (Fig. 7c and Fig. 7d). Nevertheless, a slight softening was noticeable in the low-frequency band when acceleration rose. An approximate 5 to 10% decrease in stiffness modulus was observed when increasing the acceleration from 10 to 20 m/s². Measurements at 5 m/s² were too noisy to exhibit significant differences.

Fig. 8a illustrates the effect of grip force on dissipated power at fixed acceleration and prestress. Fig. 8b shows the influence of prestress on dissipated power at fixed acceleration and grip force. Dissipated power decreased with an approximate constant slope of $-10 \, \mathrm{dB/octave}$. In other words, when frequency doubled, dissipated power was divided by three. Within the modulus-local-extreme frequency range, dissipation decreased a little more for several hundred Hz. Up to 80 Hz or so, 40% grip dissipated four to six times more power than 0% grip, demonstrating its greatest impact. The ratio dropped to two from around 300 Hz and remained stable. In parallel, differences between grip forces fell significantly. Prestress shifted curves with an almost constant value over frequency. Intermediate loading dissipated 1.5 times more power than the lowest, and the highest 2.5 times more.

3.4. Cross analysis over measurements

Fig. 9 shows the evolution of all measured physical quantities with grip force. All quantities were normalised by their no-grip value. It demonstrated that the longitudinal modulus increased the most with grip, being eight times higher at 40% than at 0%, whereas transverse modulus exhibited the smallest

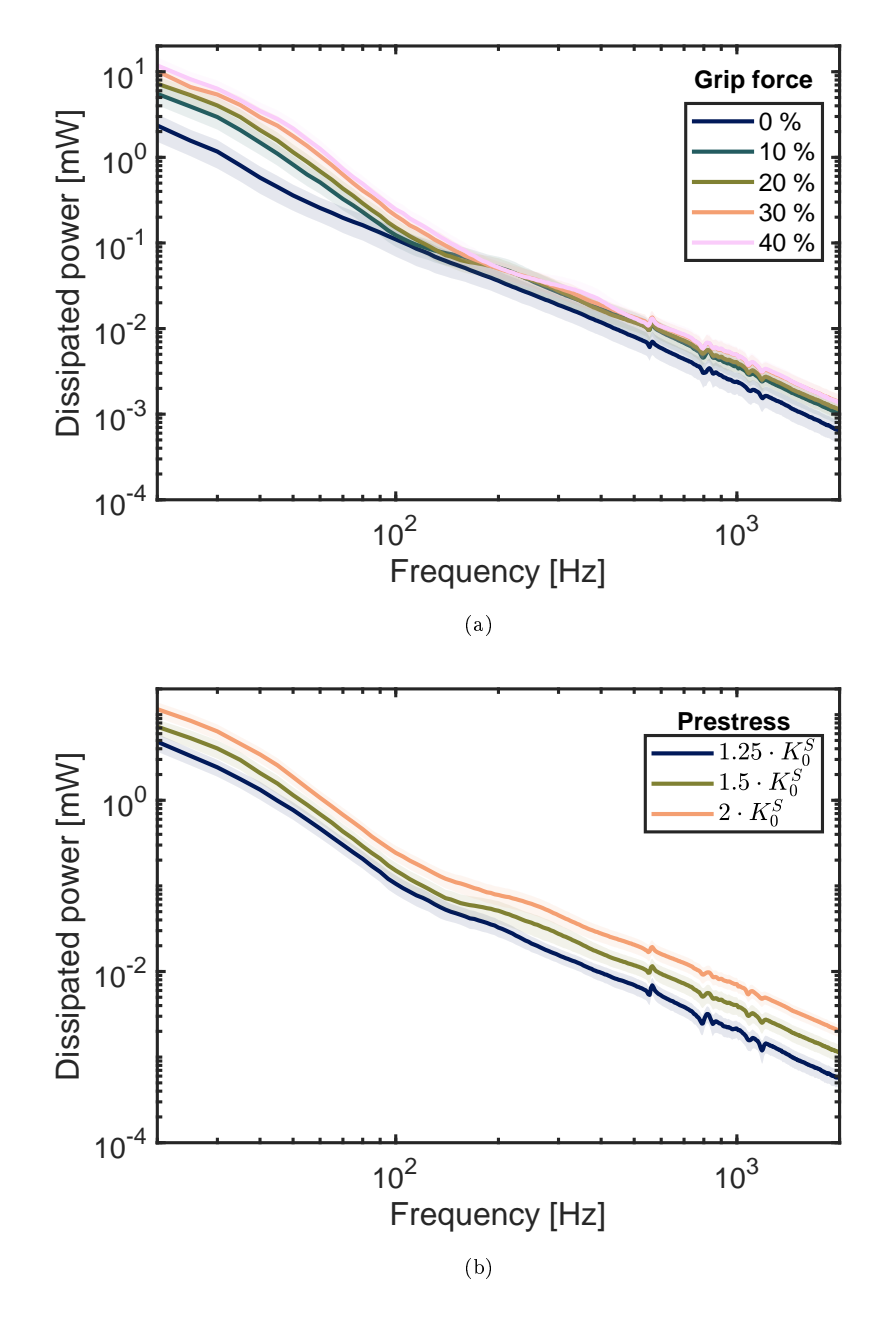


FIGURE 8 – (a) effect of grip force on dissipated power averaged among volunteers at acceleration = $20 \,\mathrm{m/s^2}$ and prestress = $1.5 \cdot K_s^0$; (b) effect of prestress on dissipated power averaged among volunteers at acceleration = $20 \,\mathrm{m/s^2}$ and grip force = 20%; transparent patches are 95%-confidence intervals.

evolution with a ratio of nearly 3. Static and dynamic stiffness were multiplied by six with gripping and followed an almost identical and quasi-linear increase (linear regression was computed over the subject-averaged modulus and exhibited R^2 -value > 0.99). For each volunteer, cross-correlations were computed between each item of data calculated in Fig. 9. It demonstrated that grip effect was highly correlated between measurement techniques; however, longitudinal and transverse moduli exhibited lower R^2 -values (Table 1).

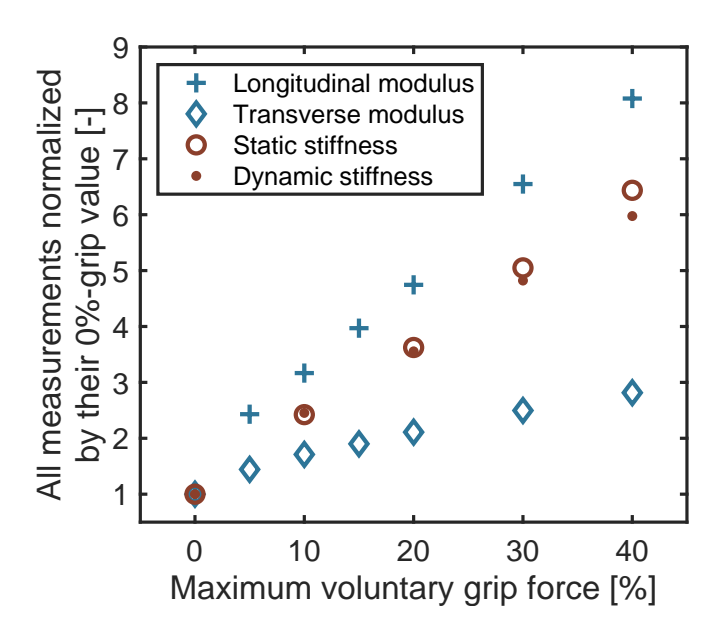


FIGURE 9 – Effect of grip on : longitudinal and transverse shear moduli, initial static stiffness (at 0-mm-indenter displacement), modulus of the dynamic stiffness modulus at 20 Hz averaged over acceleration and prestress; all data are normalized by their 0%-grip value.

Table 1 – Cross-correlation R^2 calculation among volunteers

	Mean	Standard deviation
Longitudinal modulus - Transverse modulus	0.79	0.27
Longitudinal modulus - Static stiffness	0.92	0.08
Static stiffness - Dynamic stiffness modulus	0.91	0.10

4. Discussion

This study aimed to characterise the mechanical influence of gripping on the activation of hand intrinsic muscles in order to enhance the understanding of vibration transmission within the hand. To this end, a specific apparatus was developed to qualify the hyperelasticity, the viscoelasticity and the anisotropy of the FDI muscle with gripping. Using quasi-static indentation, DMA and ultrasound elastography, measurements were conducted on a cohort of 27 volunteers. These assessments revealed that the mechanical behaviour of the muscle was significantly influenced by gripping. The principal findings indicated an increase in muscle anisotropy and stiffness with gripping. The stiffening of the tissues was evidenced by an elevation in static stiffness, dynamic stiffness, and shear modulus, all of which were correlated. Additionally, the quasi-static and dynamic mechanical tests demonstrated that the effects of grip depended on the level of deformation and frequency, respectively.

Focusing on shear wave elastography measurements obtained by SSI technique, our findings demonstrated a quasi-linear relationship between the longitudinal shear modulus and grip force (Fig. 3). Previous studies reported similar relationships between longitudinal modulus and muscle isometric contraction of the FDI muscle (Bouillard et al., 2011), the abductor digiti

minimi (Ateş et al., 2015) and the biceps brachii (Yoshitake et al., 2014, Nordez and Hug, 2010). However, in our study, the level of activation of the FDI muscle was not known because no equivalence could be established beforehand between grip level and FDI isometric contraction. Despite this, the observed linear relationship suggests that activation increased linearly with the level of gripping. The longitudinal modulus averaged over the subjects at a level of 40% grip was 77 kPa. When compared to measurements taken at 40% of maximal voluntary contraction, this value was slightly lower than those reported in other studies: 125 kPa in Yoshitake et al. (2014), 100 kPa in Ates et al. (2015), and 105 kPa in Bouillard et al. (2011). Several factors could explain this discrepancy. Firstly, the muscles studied were different. Secondly, errors in positioning the probe along the longitudinal fibre direction could reduce the measured modulus (Knight et al., 2022). Finally, gripping involves several muscles and it is likely that a given percentage of MV grip force induces a smaller contribution of the FDI muscle than more standardised movements at the same percentage, such as elbow flexion in biceps measurements or index finger abduction with the FDI muscle. At rest, our measurements were in good agreement with those of Watanabe et al. (2019) made on the FDI muscle (9.5 kPa versus 6 to 7 kPa, depending on finger flexion). Anisotropy could be evaluated by examining the ratio of the longitudinal modulus to the transverse modulus. This ratio depends on muscle activation (Gennisson et al., 2010, Ngo et al., 2024), as highlighted by our measurements, but also on stretching (Ngo et al., 2024). Therefore, direct comparison with the findings presented in previous research was difficult, because stretch levels were unknown. Nonetheless, we measured an anisotropy ratio ranging from 1.1 at 0% gripping to 4.3 at 40% gripping. These values are of a comparable magnitude to those observed in other studies (Ngo et al., 2024, Knight et al., 2022), albeit slightly lower. This could be explained by the difficulties in positioning the probe. As a poor orientation lowers longitudinal modulus, it increases transverse one (Knight et al., 2022). This phenomenon was particularly plausible given the difficulty of measuring in the transverse direction due to the small size of the FDI muscle.

The hyperelastic behaviour of the biological tissues studied was highlighted by the non-linear relationship between reaction force and indenter penetration, with gradual stiffening occurring with increased deformation. Comparative analyses with other studies were not straightforward due to the influence of testing location (variations in skin properties and subcutaneous structure) and instrumental conditions (shape and material of the indenter). Nevertheless, indentation studies on the biceps (Clemen et al., 2017), thigh (Fougeron et al., 2020), finger (Noël, 2017b) and FDI muscle (Yielder et al., 2007) demonstrated similar behaviours and comparable magnitudes. By analogy with stress-strain curves of skin tissue, the initial region of low stiffness is likely to represent the response of the elastin fibre, while the second region, where the medium gradually stiffens, may correspond to the straightening of the collagen fibre (Maurel et al., 2014). A third phase with high linear stiffness occurs at high strain, but was visible for only a few subjects. There is no simple equivalence between strain and penetration due to the complex structure of the medium. We could hypothesise that even with significant penetration, the medium may not have deformed enough to exhibit this behaviour. This hypothesis is supported by the absence of bones below the tested tissues,

thus limiting the compression—in contrast to studies where the third phase was clearly noticeable (Noël, 2017b, Fougeron et al., 2020). The calculation of the equivalent Young's modulus of contact could facilitate the integration of the shape of the indenter into the comparison of results. However, this necessitates the formulation of new assumptions regarding contact. According to Johnson (1985), however, calculation for 0\% grip measurements yielded an apparent Young's modulus that increased from 35 to 41 kPa between 1 and 4 mm. In the same displacement interval, Pailler-Mattei et al. (2008) reported values on the upper arm ranging from 13 kPa to 18 kPa, exhibiting a similar convex shape. The observed increase in Young's modulus with displacement may be indicative of the indenter deforming a stiffer layer at greater depths, namely the muscle. The observed shift between curves with increased grip was consistent with the findings reported by Clemen et al. (2017) and Fougeron et al. (2020). The intermediate elevation between longitudinal and transverse elastography measurements was coherent, given that the indenter induced shear in all directions. The high correlation between longitudinal shear modulus and quasi-static indentation indicated that both measurement techniques are similarly impacted by gripping.

To date, no studies have quantified muscular contraction in vivo using DMA. However, we found that, at 40 Hz, dynamic stiffness ranged from 0.31 N/mm, with the lowest prestress and grip, to 4.1 N/mm, with the highest. By contrast, Boyer et al. (2007) reported an average value of 0.094 N/mm for the upper arm skin at 40 Hz, but with a very low prestress (0.2 mm of indenter penetration). Furthermore, Noël (2017b) reported values for phalanx tissues ranging from 5 to 25 N/mm, which increased with prestress;

yet Noël's study employed a larger cylindrical indenter and a higher overall prestress. With regard to the effect of gripping, the identical evolution of dynamic and static stiffness, in conjunction with the high correlation between measurement techniques, provides evidence that the device was well suited to discriminating the effects of gripping. Although the standardised mechanical impedance measured on a vibrating handle exhibits considerable variability between studies, they concur that gripping exerts a significant influence on it, spanning approximately from 25 to 500 Hz (Lindenmann et al., 2022), in accordance with our findings. It is not possible to make a complete analogy with rheological theory or spring-mass-damper systems, as the phase angle does not align with those systems. However, insights can be gained from such analogies to facilitate an understanding of the dynamic behaviour of the system. Two main hypotheses have been proposed to explain the different stages separated by local minima of the dynamic stiffness. Firstly, from a rheological perspective, the initial plateau of the modulus could correspond to an amorphous polymer rubber plateau, in which the behaviour is governed by the long-chain molecules. The asymptotic behaviour would correspond to the glassy region, which is governed by limited local molecular motion of side groups. Between these two regions would be the transition region, in which polymers chains rearrange. In this region, the two peaks observed in the phase argument could correspond to the two so-called α and β peaks (Lakes, 2009). From the standpoint of structural mechanics, the aforementioned minima could also represent local resonances, particularly when taking into account the findings of harmonic simulations that exhibited resonances of muscles in the 200-400 Hz frequency range (Noël et al., 2022, Vauthier

et al., 2023). It can be reasonably assumed that an increase in clamping stiffness will result in an increase in the frequency of these peaks. This is due to the fact that Young's modulus increases, while mass remains unchanged. At frequencies approaching the upper limit of the frequency range, the effect of the indenter vibration was likely to become highly localised, primarily reflecting the properties of the skin, although the muscle continued to act as a boundary condition, varying with gripping pressure and influencing the overall response. In order to provide a rough estimation of propagation distance, it can be assumed that when neglecting the modulus of the indenter and considering the tissues as incompressible, the overall Young's modulus (of undifferentiated skin, flesh and muscle) at a displacement of 1 mm was 131 kPa, which corresponds to a wavelength of 5.7 mm when measured at 2000 Hz (Kinsler, 2000). The near-identical elevation of dynamic stiffness modulus at low frequency to quasi-static modulus, coupled with a high correlation between them, provides valuable insight into the capacity of our dynamic apparatus to evaluate the effects of grip.

Nevertheless, a number of limitations arose from our experiments. The primary limitation result from our cohort-oriented approach. Indeed, given our objective of encompassing all workers exposed to vibrations, our analysis was only conducted on the entire cohort, without extracting clusters or volunteers. The aggregation of measurements across the entire cohort provided insights into the consistency in mechanical behaviour between individuals. At the same time, however, the aggregated data also obscured certain individual differences. In particular, the utilisation of the FDI muscle for gripping differed between individuals. The primary mechanism of gripping is phalanx

flexion, in which the FDI muscle is not involved (Watanabe et al., 2019). This is followed by secondary movements such as abduction of the index finger done with the FDI muscle. The measurements revealed important discrepancies in amplitude between individuals. While these discrepancies were consistent across the three measured quantities (Tab. 1), they were not correlated with the maximum grip force. It is possible that these differences were due to a more or less predominant use of the FDI muscle for gripping. As a result, we could not conclude if the differences observed were the result of either variability of the mechanical behaviour of tissues, or volunteer individual grip strategy. The cohort approach also oriented our experimental protocol towards robustness and high repeatability. To a certain extent, however, this approach may be perceived as having limited the precision of our measurements. For instance, in the quasi-static measurements, the exponential fit suitably represented the shape of the curve on the entire range; but it tended to overestimate the stiffness in very low penetration and poorly reflected the initial quasi-linear behaviour of tissues. Also, we were constrained to limit the number of tested parameters and repetitions so that the duration of the protocol (half a day) could be easily manageable by the volunteers. Although acceleration demonstrated a weak effect on dynamic measurements, repeatability within subjects and a wider band of excitation could have consolidated conclusions.

The second major limitation may be found in how our findings might be exploited. The most likely application arising from our study would be the identification of parameters from constitutive mechanical laws, but this identification could be limited by several factors. Though our tests were complementary in order to give a complete characterisation of the muscle (hyperelasticity, viscoelasticity and anisotropy), they are not easily combinable for an identification analysis. Furthermore, even if each technique were isolated, it would remain incomplete and therefore unsuitable for fully rigorous exploitation. In the context of elastography, the assumption that the FDI muscle can be considered as a linear and transverse isotropic material necessitates the determination of two shear moduli, two Poisson's ratios and two Young's moduli. The shear moduli were obtained through measurements, while the Poisson's ratios are known through the assumption of incompressibility. The transverse Young modulus can be derived from the fundamental relationship of elasticity theory, given that the medium is isotropic in this plane in contrast to the other. On the contrary, the longitudinal Young modulus cannot be deduced directly from measurements and remains unknown. In the case of quasi-static indentation, the identification of muscle properties from contact theory may prove challenging due to the complex, multi-layered nature of the medium and the presence of additional superficial layers on the muscle. The accuracy of these deductions is highly dependent on contact conditions. With regard to this point, the friction coefficient is dependent on surface conditions or skin hydration, and even with lubrication of the contact, the friction coefficient remains almost unknown. Finally, reaction force depends heavily on the indenter's angle of incidence. The inclination of the handle was chosen to ensure that the contact surface remained orthogonal to the contact; but in practice, this was roughly horizontal as it depended on the anatomy of volunteers. With regard to the determination of viscoelastic properties, it proved impossible to estimate the storage and loss modules

due to the complex geometry of the system. This prevented relatively simple analytical identification of parameters from rheological models such as the Prony series. As a result, the primary methodology for the inverse identification of material parameters entails finite element modeling, which involves the numerical reproduction of the indentation contact. Nevertheless, Clemen et al. (2017) demonstrated that this approach is suitable even when dealing with complex constitutive laws.

5. Conclusion

The present study was initiated in response to a perceived lack of knowledge in the field of hand-arm vibration syndrome regarding the mechanical behaviour of hand intrinsic muscles during gripping. The use of quasi-static indentation, DMA and shear wave elastography in a cohort of volunteers demonstrated that gripping had a significant impact on the material properties of the FDI muscle. Our principal findings were that the FDI muscle stiffened in response to increasing grip force, with the greatest change occurring in the direction longitudinal to the muscle fibre. Additionally, stiffness demonstrated a nonlinear increase with indenter penetration and showed a pronounced dependence on excitation frequency.

The greatest influence of grip force was observed between 20 Hz and approximately 300 Hz. Furthermore, it was observed that the FDI muscle exhibited a four- to six-fold increase in mechanical power dissipation between 20 and 80 Hz when the handle was gripped using the maximum instructed force, in comparison to a no-grip condition. Nevertheless, the *in vivo* measurements exhibited important inter-individual variability, which was attributed

to differences in both anatomy and gripping strategies between volunteers. Additionally, although these measurements were as comprehensive as possible, they remain incomplete in order to provide a solution that is ready to use in the identification of constitutive laws. That said, this study represents a preliminary investigation into the properties of hand muscles during gripping. Its findings demonstrate that this subject is of the utmost importance and that further research should be pursued in this area. We hope that our findings will contribute to the development of more accurate numerical models and to the improvement of strategies for the prevention of hand-arm vibration syndrome.

6. Acknowledgements

This work has been achieved in the frame of the EIPHI Graduate school (contract ANR-17-EURE-0002).

Références

- Adewusi, S.A., Rakheja, S., Marcotte, P., Boileau, P.E., 2008. On the discrepancies in the reported human hand-arm impedance at higher frequencies. International Journal of Industrial Ergonomics 38, 703-714. doi:10.1016/j.ergon.2007.12.004.
- Ateş, F., Hug, F., Bouillard, K., Jubeau, M., Frappart, T., Couade, M., Bercoff, J., Nordez, A., 2015. Muscle shear elastic modulus is linearly related to muscle torque over the entire range of isometric contraction intensity. Journal of Electromyography and Kinesiology 25, 703–708. doi:10.1016/j.jelekin.2015.02.005.
- Bilbo, J.T., Stern, P.J., 1986. The first dorsal interesseous muscle: An anatomic study. Journal of Hand Surgery 11, 748–750. doi:10.1016/S0363-5023(86)80027-2.
- Bouillard, K., Nordez, A., Hug, F., 2011. Estimation of individual muscle force using elastography. PLoS ONE 6. doi:10.1371/journal.pone.0029261.
- Bovenzi, M., 1990. Medical aspects of the hand-arm vibration syndrome. International Journal of Industrial Ergonomics 6, 61–73. doi:10.1016/0169-8141(90)90051-3.
- Boyer, G., Zahouani, H., Le Bot, A., Laquieze, L., 2007. In vivo characterization of viscoelastic properties of human skin using dynamic microindentation, in: 2007–29th Annual International Conference of the IEEE

- Engineering in Medicine and Biology Society, pp. 4584–4587. doi:10.1109/IEMBS.2007.4353360.
- Burström, L., Lundström, R., 1988. Mechanical energy absorption in human hand-arm exposed to sinusoidal vibration. International Archives of Occupational and Environmental Health 61, 213–216. doi:10.1007/BF00381021.
- Chatelin, S., Oudry, J., Périchon, N., Sandrin, L., Allemann, P., Soler, L., Willinger, R., 2011. In vivo liver tissue mechanical properties by transient elastography: Comparison with dynamic mechanical analysis. Biorheology 48, 75–88. doi:10.3233/BIR-2011-0584.
- Chetter, I.C., Kent, P.J., Kester, R.C., 1997. The hand arm vibration syndrome: A review. Cardiovascular Surgery 6, 1–9. doi:10.1016/S0967-2109(97)00090-2.
- Clemen, C.B., Benderoth, G.E.K., Schmidt, A., Hübner, F., Vogl, T.J., Silber, G., 2017. Human skeletal muscle behavior in vivo: Finite element implementation, experiment, and passive mechanical characterization. Journal of the Mechanical Behavior of Biomedical Materials 65, 679–687. doi:10.1016/j.jmbbm.2016.09.030.
- Dong, R.G., Welcome, D.E., McDowell, T.W., Wu, J.Z., 2008. Analysis of handle dynamics-induced errors in hand biodynamic measurements. Journal of Sound and Vibration 318, 1313–1333. doi:10.1016/j.jsv.2008.04.038.

- Fougeron, N., Rohan, P.Y., Haering, D., Rose, J.L., Bonnet, X., Pillet, H., 2020. Combining Freehand Ultrasound-Based Indentation and Inverse Finite Element Modeling for the Identification of Hyperelastic Material Properties of Thigh Soft Tissues. Journal of Biomechanical Engineering 142. doi:10.1115/1.4046444.
- Gennisson, J.L., Deffieux, T., Fink, M., Tanter, M., 2013. Ultrasound elastography: Principles and techniques. Diagnostic and Interventional Imaging 94, 487–495. doi:10.1016/j.diii.2013.01.022.
- Gennisson, J.L., Deffieux, T., Macé, E., Montaldo, G., Fink, M., Tanter, M., 2010. Viscoelastic and anisotropic mechanical properties of in vivo muscle tissue assessed by supersonic shear imaging. Ultrasound in Medicine and Biology 36, 789–801. doi:10.1016/j.ultrasmedbio.2010.02.013.
- Ghatas, M.P., Khan, M.R., Gorgey, A.S., 2021. Skeletal muscle stiffness as measured by magnetic resonance elastography after chronic spinal cord injury: A cross-sectional pilot study. Neural Regeneration Research 16, 2486–2493. doi:10.4103/1673-5374.313060.
- Gras, L.L., Mitton, D., Viot, P., Laporte, S., 2012. Hyper-elastic properties of the human sternocleidomastoideus muscle in tension. Journal of the Mechanical Behavior of Biomedical Materials 15, 131–140. doi:10.1016/j.jmbbm.2012.06.013.
- Griffin, M., 2012a. Handbook of Human Vibration. Elsevier Science.
- Griffin, M.J., 2012b. Frequency-dependence of Psychophysical and Physio-

- logical Responses to Hand-transmitted Vibration. Industrial Health 50, 354-369. doi:10.2486/indhealth.MS1379.
- Hirt, B., Seyhan, H., Wagner, M., Zumhasch, R., 2017. Hand and Wrist Anatomy and Biomechanics: A Comprehensive Guide. Thieme, Stuttgart; New York.
- Infantolino, B.W., Challis, J.H., 2010. Architectural properties of the first dorsal interosseous muscle. Journal of Anatomy 216, 463–469. doi:10.1111/j.1469-7580.2009.01196.x.
- ISO 10068:2012, 2012. Mechanical vibration and shock Mechanical impedance of the human hand-arm system at the driving point. International Organization for Standardization, Geneva, Switzerland. URL: https://www.iso.org/standard/53714.html.
- Johnson, K.L., 1985. Contact Mechanics. Cambridge University Press, Cambridge. doi:10.1017/CB09781139171731.
- Kearney, S.P., Khan, A., Dai, Z., Royston, T.J., 2015. Dynamic viscoelastic models of human skin using optical elastography. Physics in Medicine & Biology 60, 6975. doi:10.1088/0031-9155/60/17/6975.
- Khaothong, K., 2010. In Vivo Measurements of the Mechanical Properties of Human Skin and Muscle by Inverse Finite Element Method Combined with the Indentation Test, in: Lim, C.T., Goh, J.C.H. (Eds.), 6th World Congress of Biomechanics (WCB 2010). August 1-6, 2010 Singapore, Springer Berlin Heidelberg, Berlin, Heidelberg, pp. 1467–1470.

- Kinsler, L.E., 2000. Fundamentals of Acoustics. 4th ed ed., Wiley, Hoboken, NJ.
- Knight, A.E., Trutna, C.A., Rouze, N.C., Hobson-Webb, L.D., Caenen, A., Jin, F.Q., Palmeri, M.L., Nightingale, K.R., 2022. Full Characterization of in vivo Muscle as an Elastic, Incompressible, Transversely Isotropic Material Using Ultrasonic Rotational 3D Shear Wave Elasticity Imaging. IEEE Transactions on Medical Imaging 41, 133–144. doi:10.1109/TMI.2021.3106278.
- Krajnak, K., Riley, D.A., Wu, J., McDowell, T., Welcome, D.E., Xu, X.S., Dong, R.G., 2012. Frequency-dependent effects of vibration on physiological systems: Experiments with animals and other human surrogates. Industrial Health 50, 343–353. doi:10.2486/indhealth.ms1378.
- Lakes, R.S., 2009. Viscoelastic Materials. Cambridge University Press.
- Lindenmann, A., Schröder, T., Germann, R., Gwosch, T., Matthiesen, S., 2022. Effect of high level grip-and push force and elevated arm posture on the zh-axis hand-arm impedance. International Journal of Industrial Ergonomics 92, 103375. doi:10.1016/j.ergon.2022.103375.
- Liu, S., Xu, H., Shang, Y., Jiang, W., Dong, J., 2020. Finite element modal analysis and harmonic response analysis of human arm grasping model. Computer Methods in Biomechanics and Biomedical Engineering 23, 1082–1093. doi:10.1080/10255842.2020.1787392.
- Lundström, R., 1984. Local vibrations-mechanical impedance of the human

- hand's glabrous skin. Journal of Biomechanics 17, 137–144. doi:10.1016/0021-9290(84)90131-3.
- Maurel, W., Wu, Y., Magnenat Thalmann, N., Thalmann, D., 2014. Biomechanical Models for Soft Tissue Simulation. ESPRIT Basic Research Series. aufl. 1998 ed., Springer Berlin, Berlin.
- Morrow, D.A., Haut Donahue, T.L., Odegard, G.M., Kaufman, K.R., 2010. Transversely isotropic tensile material properties of skeletal muscle tissue. Journal of the Mechanical Behavior of Biomedical Materials 3, 124–129. doi:10.1016/j.jmbbm.2009.03.004.
- Ngo, H.H.P., Andrade, R., Brum, J., Benech, N., Chatelin, S., Loumeaud, A., Frappart, T., Fraschini, C., Nordez, A., Gennisson, J.L., 2024. In plane quantification ofin vivomuscle elastic anisotropy factor by steered ultrasound pushing beams. Physics in Medicine and Biology 69. doi:10.1088/1361-6560/ad21a0.
- Noël, C., 2011. Acceleration mapping and local biodynamic response of hand gripping a vibrating handle by using laser scanning vibrometer, in: 46th UK Conference on Human Response to Vibration, Health and Safety Laboratory and the Health and Safety Executive, Buxton. pp. 173–184.
- Noël, C., 2017a. Influence des efforts de poussée-préhension et des gants anti-vibratiles sur le transfert des vibrations à la main. Hygiène et sécurité du travail 247, 48-54. URL: https://www.inrs.fr/dms/inrs/CataloguePapier/HST/TI-NT-50/nt50.pdf. [in French].

- Noël, C., 2017b. Measuring dynamic stiffnesses of preloaded distal phalanges in vibration Test bench validation and parameter study. International Journal of Industrial Ergonomics 59, 64–79. doi:10.1016/j.ergon.2017.03.006.
- Noël, C., 2018. A three-dimensional visco-hyperelastic FE model for simulating the mechanical dynamic response of preloaded phalanges. Medical Engineering and Physics 61, 41–50. doi:10.1016/j.medengphy.2018.08.007.
- Noël, C., Settembre, N., Reda, M., Jacquet, E., 2022. A Multiscale Approach for Predicting Certain Effects of Hand-Transmitted Vibration on Finger Arteries. Vibration 5, 213–237. doi:10.3390/vibration5020014.
- Nordez, A., Hug, F., 2010. Muscle shear elastic modulus measured using supersonic shear imaging is highly related to muscle activity level. Journal of Applied Physiology 108, 1389–1394. doi:10.1152/japplphysiol.01323.2009.
- Pailler-Mattei, C., Bec, S., Zahouani, H., 2008. In vivo measurements of the elastic mechanical properties of human skin by indentation tests. Medical Engineering & Physics 30, 599–606. doi:10.1016/j.medengphy.2007.06.011.
- Pan, D., Xu, X.S., Welcome, D.E., McDowell, T.W., Warren, C., Wu, J., Dong, R.G., 2018. The relationships between hand coupling force and vibration biodynamic responses of the hand-arm system. Ergonomics 61, 818–830. doi:10.1080/00140139.2017.1398843.

- Riordan, D.C., 1995. A walk through the anatomy of the hand and forearm.

 Journal of Hand Therapy: Official Journal of the American Society of

 Hand Therapists 8, 68–78. doi:10.1016/s0894-1130(12)80302-4.
- Royer, D., Gennisson, J.L., Deffieux, T., Tanter, M., 2011. On the elasticity of transverse isotropic soft tissues (L). The Journal of the Acoustical Society of America 129, 2757–2760. doi:10.1121/1.3559681.
- Schafer, R.W., 2011. What Is a Savitzky-Golay Filter? [Lecture Notes]. IEEE Signal Processing Magazine 28, 111–117. doi:10.1109/MSP.2011.941097.
- Vauthier, S., Noël, C., Settembre, N., Ngo, H.H.P., Gennisson, J.L., Chambert, J., Foltête, E., Jacquet, E., 2023. Factoring Muscle Activation and Anisotropy in Modelling Hand-Transmitted Vibrations: A Preliminary Study, in: ICHAV 2023, MDPI. p. 12. doi:10.3390/proceedings2023086012.
- Wang, Z., Qiu, Y., Zheng, X., Hao, Z., Liu, C., 2022. Biomechanical models of the hand-arm system to predict the hand gripping forces and transmitted vibration. International Journal of Industrial Ergonomics 88, 103258. doi:10.1016/j.ergon.2021.103258.
- Watanabe, Y., Iba, K., Taniguchi, K., Aoki, M., Sonoda, T., Yamashita, T., 2019. Assessment of the Passive Tension of the First Dorsal Interosseous and First Lumbrical Muscles Using Shear Wave Elastography. The Journal of Hand Surgery 44, 1092.e1–1092.e8. doi:10.1016/j.jhsa.2019.01.016.
- Wheatley, B.B., Morrow, D.A., Odegard, G.M., Kaufman, K.R., Haut Donahue, T.L., 2016. Skeletal muscle tensile strain dependence: Hypervis-

- coelastic nonlinearity. Journal of the Mechanical Behavior of Biomedical Materials 53, 445–454. doi:10.1016/j.jmbbm.2015.08.041.
- Wu, J.Z., Dong, R.G., Warren, C.M., Welcome, D.E., McDowell, T.W., 2014.
 Analysis of the effects of surface stiffness on the contact interaction between a finger and a cylindrical handle using a three-dimensional hybrid model. Medical Engineering and Physics 36, 831–841. doi:10.1016/j.medengphy.2014.03.007.
- Wu, J.Z., Dong, R.G., Welcome, D.E., 2006. Analysis of the point mechanical impedance of fingerpad in vibration. Medical Engineering & Physics 28, 816–826. doi:10.1016/j.medengphy.2005.11.013.
- Wu, J.Z., Welcome, D.E., McDowell, T.W., Xu, X.S., Dong, R.G., 2017. Modeling of the interaction between grip force and vibration transmissibility of a finger. Medical Engineering and Physics 45, 61–70. doi:10.1016/j.medengphy.2017.04.008.
- Yielder, P., Gutnik, B., Kobrin, V.I., Leaver, J., Guo, W., 2007. Viscoelastic properties of a skin-and-muscle compartment in the right and the left hands. Biophysics 52, 220–226. doi:10.1134/S0006350907020133.
- Yoshitake, Y., Takai, Y., Kanehisa, H., Shinohara, M., 2014. Muscle shear modulus measured with ultrasound shear-wave elastography across a wide range of contraction intensity. Muscle & Nerve 50, 103–113. doi:10.1002/mus.24104.
- Zahouani, H., Pailler-Mattei, C., Sohm, B., Vargiolu, R., Cenizo, V., Debret, R., 2009. Characterization of the mechanical properties of a dermal equiva-

lent compared with human skin in vivo by indentation and static friction tests. Skin Research and Technology 15, 68–76. doi:10.1111/j.1600-0846.2008.00329.x.